IKP-MS-92/0101

Recent Results from the WA80 Experiment at CERN

WA80 Collaboration

INSTITUT FÜR KERNPHYSIK
UNIVERSITÄT MÜNSTER

Recent Results from the WA80 Experiment at CERN *

WA80 Collaboration

K.H. Kampert[4], R. Albrecht[1], T.C. Awes[5], P. Beckmann[4,a], F. Berger[4], M. Bloomer[2], D. Bock[4], R. Bock[1], G. Claesson[3], G. Clewing[4], R. Debbe[6], L. Dragon[4,b], A. Eklund[3], R.L. Ferguson[5], S. Fokin[7], A. Franz[5,a], S. Garpman[3], R. Glasow[4], H.Å. Gustafsson[3], H.H. Gutbrod[1], O. Hansen[6], M. Hartig[4], G. Hölker[4], J. Idh[3], M. Ippolitov[7], P. Jacobs[2], K. Karadjev[7], B.W. Kolb[1], A. Lebedev[7], H. Löhner[4,c], I. Lund[1,c], V. Manko[7], B. Moskowitz[6], F.E. Obenshain[5], A. Oskarsson[3], I. Otterlund[3], T. Peitzmann[4], F. Plasil[5], A.M. Poskanzer[2], M. Purschke[4], H.G. Ritter[2], B. Roters[4], S. Saini[5], R. Santo[4], H.R. Schmidt[1], R. Schmidt[4], S.P. Sørensen[5,d], K. Steffens[4], P. Steinhaeuser[4], E. Stenlund[3], D. Stüken[4], A. Vinogradov[7], H. Wegener[6], and G.R. Young[5]

1. *Gesellschaft für Schwerionenforschung, D-6100 Darmstadt, Fed. Rep. of Germany*
2. *Lawrence Berkeley Laboratory, Berkeley, California 94720, USA*
3. *University of Lund, S-22362 Lund, Sweden*
4. *University of Münster, D-4400 Münster, Fed. Rep. of Germany*
5. *Oak Ridge National Laboratory, Oak Ridge, Tennessee 37831, USA*
6. *Brookhaven National Laboratory, Upton, New York 11973, USA*
7. *Kurchatov Institute of Atomic Energy, Moscow 123182, USSR*

a. *now at: CERN, CH-1211 Geneva 23, Switzerland*
b. *now at: Mercedes-Benz, D-7000 Stuttgart, Fed. Rep. of Germany*
c. *now at: KVI, University of Groningen, NL-9747 AA Groningen, Netherlands*
d. *University of Tennessee, Knoxville, Tennessee 37996, USA*

Abstract

Results from the WA80 experiment on systematics of global observables, $dE_T/d\eta$ and $dN_{ch}/d\eta$, as well as on spectra of identified particles are presented. Special attention is given to the target fragmentation region where two-pion correlations and proton distributions have been measured. Incorporation of strong rescattering phenomena into string models is found to provide a good description of most experimental data. Deviations to this are pointed out. The present status of the $\gamma_{thermal}/\pi^0$ ratio as a signal of the quark gluon plasma is discussed.

1 Introduction

The aim of high-energy heavy-ion collisions studied at the SPS and AGS accelerators is to investigate nuclear matter under conditions of extremely high densities and temperatures. Theoretical calculations predict that under such conditions hadronic matter might undergo a phase-transition to a new form of matter, the quark-gluon plasma

*Invited Talk at the Ninth International Conference on Ultra-Relativistic Nucleus-Nucleus Collisions Quark Matter '91
November 11–15, 1991, Gatlinburg, Tennesse, USA

(QGP), in which quarks and gluons are deconfined over an extended volume [1]. A broad spectrum of possible plasma signatures has been suggested and was discussed on this conference. Unfortunately, a common characteristic of most of these signatures is the necessity to distinguish them from the large background created by ordinary hadronic processes. A thorough understanding of the reaction mechanism is, therefore, an important prerequisite in any search for the QGP. Besides the time evolution of the reaction system, which is a central focus in this field of research, one has to learn about the interaction of produced particles with their high density nuclear environment as well as among produced particles themselves.

To address such questions, we will present results from a comprehensive analysis of p-, ^{16}O-, and ^{32}S-induced reactions at bombarding energies of 4.9, 60, and 200 AGeV across a large variety of target nuclei. Quantities like the transverse energy pseudorapidity density, $dE_T/d\eta$, and the charged particle density, $dN_{ch}/d\eta$, have been proven to be valuable tools for obtaining an understanding of the reaction mechanism. We will discuss these observables in section 3. The investigation of the target fragmentation region provides a unique tool to extract detailed information about rescattering phenomena. In hadron-nucleus interactions the target nucleons can serve as "detectors" for reaction products at distances and time scales not accessible with macroscopic detectors. Thus, we study rescattering phenomena of produced particles with "cold" matter in section 4.1 by employing the Plastic-Ball detector which is capable of identifying pions and protons. Two pion correlations, suggested to carry further information about the space-time evolution of the collision, will be discussed in section 4.2. Having provided experimental evidence for a strong excitation of the target matter, we will show in section 5 that rescattering effects as incorporated in the string model VENUS 3.07, allow a quantitative description of high p_T neutral pion spectra measured at midrapidity in central collisions of O, S + nucleus. The analysis of thermal photon production in O + Au and S + Au will be reported in section 6.

2 Experimental Setup

The experiments were performed with the WA80 experimental setup [2] at the CERN SPS between 1986 and 1990. In spring 1990 the setup has been considerably modified to improve the acceptance for π^0 and η-mesons. A sketch of the new experimental layout is depicted in Fig. 1.

The data presented here were obtained with the detectors and configurations as described briefly below:
The Zero-Degree Calorimeter (ZDC) [3] covers the pseudorapidity of $\eta > 6.0$ and is used for impact parameter selection. The Mid-Rapidity Calorimeter (MIRAC) [4] measures the transverse energy with full azimuthal coverage in $2.4 \leq \eta \leq 5.5$. For $1.6 \leq \eta \leq 2.4$ the azimuthal coverage varied from 10% to 100%. The lead-glass calorimeter wall (Saphir + Tower I + Tower II) [5] comprises 3798 modules covering 2.2π in azimuth and $2.1 \leq \eta \leq 2.9$ in pseudorapidity. The distance to the target is 9.0 m. (1986-1989: 1278 modules at 3.4 m and $1.5 \leq \eta \leq 2.1$). The front face of the lead-glass wall is fully covered by two layers of Iarocchi streamer tube detectors with pad readout [6]. Due to

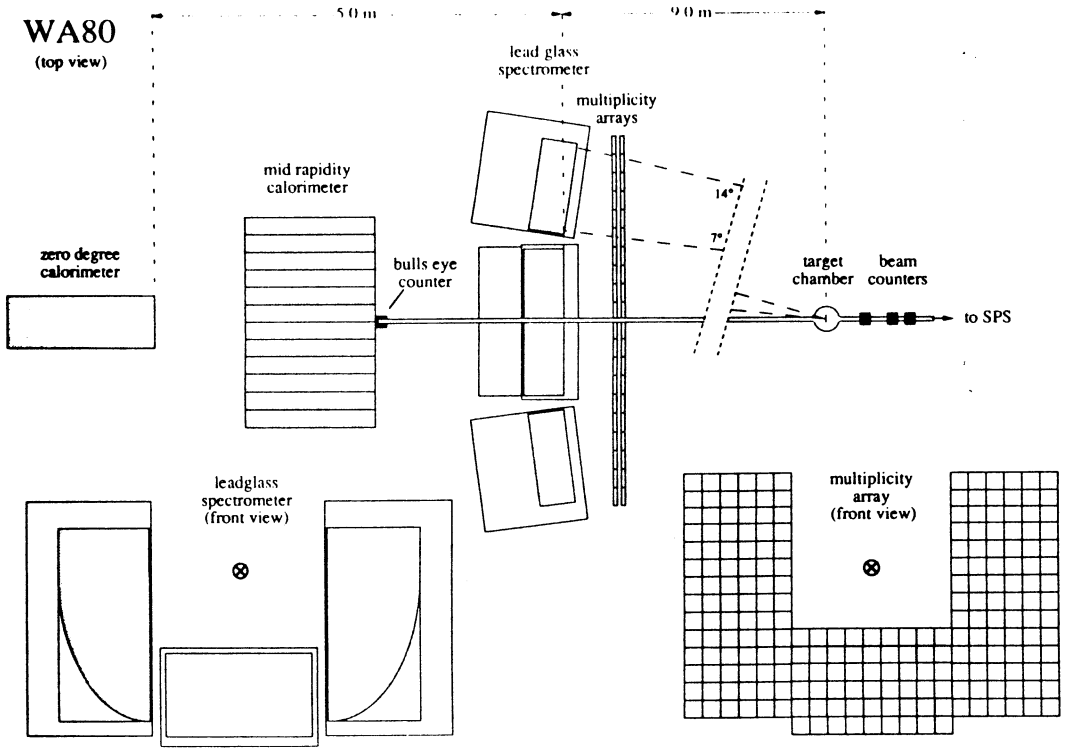

Figure 1: Sketch of the WA80 experimental setup as of 1990

the high granularity (21k + 21k pads) and efficiency ($\varepsilon > 93\%$) the detector can be used both as a charged particle veto detector for the photon calorimeter as well as a charged particle tracking detector in its own. The Plastic-Ball detector [7] is an azimuthally symmetric array of 655 ΔE-E telescopes allowing the identification of light baryons and positive pions in the pseudorapidity region $-1.7 \leq \eta \leq 1.0$.

The minimum bias trigger condition was defined by requiring less than 88% of the full beam energy recorded by the ZDC and at least one charged particle recorded by the multiplicity arrays in the interval $1.3 \leq \eta \leq 4.4$.

3 Global Observables

3.1 Systematics of $dE_T/d\eta$ Distributions

In this section we will discuss the dependence of the $dE_T/d\eta$ distributions on impact parameter, projectile- and target mass, and beam energy. As an example we show in Fig. 2 the $dE_T/d\eta$ distributions in 200 AGeV ^{32}S-induced minimum bias collisions on various target nuclei. The effects of increasing target mass are very similar to decreasing the impact parameter for a given system and are manifested in an increasing height, decreasing peak position, and narrower width of the distributions. Superimposed to the data are results from Gaussian fits. The results of the fits are in general very good (χ^2/ndf $\approx$ 0.3-0.5), so that the three free parameters, $dE_T/d\eta|_{max}$, $\overline{\eta}$, and σ_n exhaust the full information content in the measured distributions.

Substantial interest has been devoted to the mass- and energy-scaling of the $dE_T/d\eta$

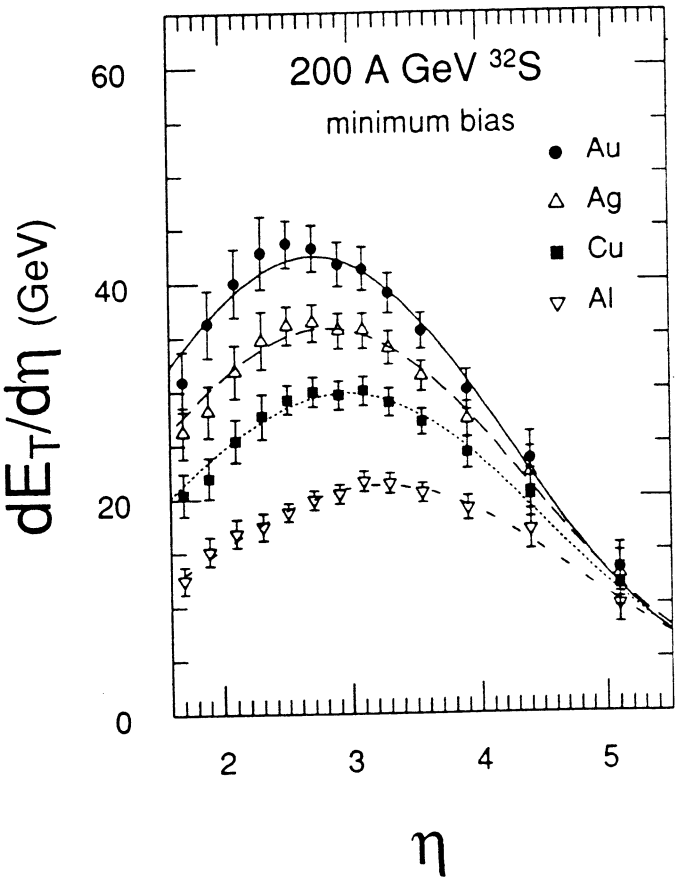

Figure 2: Target dependence of $dE_T/d\eta$ in 200 AGeV ^{32}S-induced minimum bias collisions.

-distributions. Universal scaling laws have been difficult to obtain as long as the scaling variables have been chosen as the projectile- and target-masses, A_p and A_t. WA80 has therefore stressed the importance of incorporating the number of participant nucleons in a consistent description of high energy nuclear collisions. To present the data together with a minimum amount of model assumptions, we have chosen to discuss the data in terms of a simple participant-spectator model based on Glauber-theory. This avoids in particular any specific comparison to high energy nuclear collision Monte-Carlo models. The basic procedure in this method is to determine the impact parameter from the forward energy measured in the ZDC, and calculating the average number of projectile- and target-participants, $\overline{W}_p$ and $\overline{W}_t$, respectively, in a geometrical picture for the three different event classes chosen in the following:

$$\begin{aligned} \text{central} &\equiv & b &< R_t - R_p \\ \text{intermediate} &\equiv R_t - R_p < & b &< R_t \\ \text{peripheral} &\equiv R_t < & b &< R_{mb} \end{aligned}$$

where R_p and R_t are the projectile and target radii, $R = 1.2 \cdot A^{1/3}$, and $R_{mb} = \sqrt{\sigma_{mb}/\pi}$ with σ_{mb} being the minimum bias cross section.

Figure 3 shows the behaviour of the $dE_T/d\eta|_{max}$ and σ_n values as a function of the total number of participants, $\overline{W} = \overline{W}_p + \overline{W}_t$, for two different projectiles, five different targets, each selected for the three event classes discussed above, and for two bombarding energies (33 combinations in total). $dE_T/d\eta|_{max}$ appears to be approximately linearly proportional to the average number of participants with the coefficient of proportionality

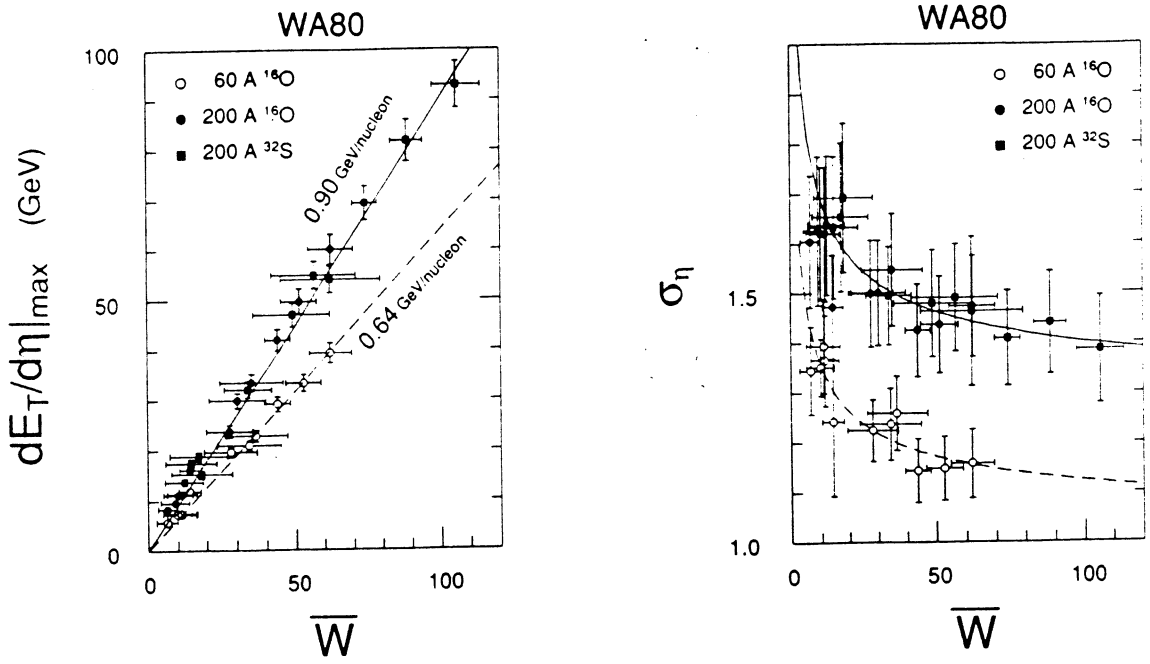

Figure 3: a) Maximum value of $dE_T/d\eta$ distributions as a function of the total average number of participants $\overline{W}$. The straight lines show linear fits through the origin to the data points at 60 and 200 AGeV, respectively. b) Standard deviation σ_n of the $dE_T/d\eta$ distributions as a function of $\overline{W}$. The solid and dashed lines represent fits according to $\sigma_n = 0.2\,(y_p - y_t)(1+\overline{W}^{-0.36})$.

equal to 0.64 and 0.90 GeV/nucleon at 60 and 200 A GeV, respectively. The increase of $dE_T/d\eta|_{max}$ in Fig. 2 is therefore a simple consequence of the increase of $\overline{W}$. The width of the $dE_T/d\eta$ distributions (Fig. 3b) becomes narrower for more central collisions and is most likely caused by an increase in stopping. The variation of the centroid $\overline{\eta}$ is more complicated and indicates a collective interaction of the projectile participants with all target participants, as may be due to the occurrence of rescattering effects, particularly for heavy targets [8].

An important result is that a symmetric description between projectile and target can easily be obtained with the participant variables $\overline{W}_p$ and $\overline{W}_t$. Based on the observation that the $dE_T/d\eta$ distributions for a particular η-value scales as a power law in both $\overline{W}_p$ and $\overline{W}_t$ a universal parametrization of $dE_T/d\eta$ is derived:

$$\frac{dE_T}{d\eta}(b) = G(\eta)\,\overline{W}_p^{\alpha(y_p-\eta)}\,\overline{W}_t^{\alpha(\eta-y_t)}$$

$$G(\eta) = \frac{N}{\sqrt{2\pi\sigma_n^2}}\exp\left\{-\frac{1}{2}\left(\frac{\eta-\eta_0}{\sigma_n}\right)^2\right\}\;;\;\; \alpha(x) = \left(1+\exp\left\{\frac{x-\eta_0}{\sigma_\alpha}\right\}\right)^{-1}$$

$G(\eta)$ can be interpreted as a Gaussian describing the $dE_T/d\eta$ distributions for nucleon-nucleon collisions. $\overline{W}^\alpha$ describes the projectile and target mass dependence, where the exponent α has been chosen as a Fermi distribution so that $dE_T/d\eta$ scales with the

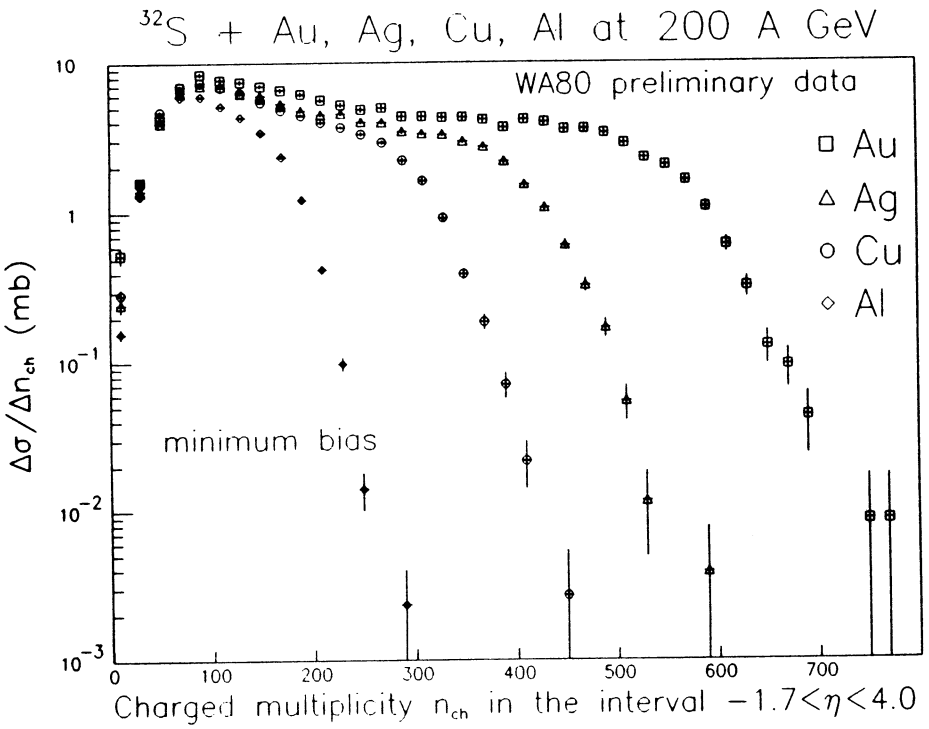

Figure 4: Multiplicity distributions of charged particles from ^{32}S + Al, Cu, Ag, and Au interactions at 200 AGeV incident energy. The pseudorapidity interval covered is $-1.7 \leq \eta \leq 4.0$.

number of target participants in the target region and is independent of the target in the projectile region. The projectile dependence is the inverse of this.

This parametrization directly relates the $dE_T/d\eta$ distributions to the physically relevant number of participants and achieves a fairly high accuracy with only five free parameters. The fit parameters are found to be

$$N = 0.41\,(y_p - y_t - 1.51)\ \text{GeV} \qquad \eta_0 = 0.51\,(y_p + y_t)$$
$$\sigma_n = 0.24\,(y_p - y_t) \qquad \sigma_\alpha = 0.12\,(y_p - y_t)$$

with y_p and y_t being the projectile and target rapidities, respectively. Within the acceptance of MIRAC we find an accuracy of better than 10% for 95% of all fitted data points.

3.2 Charged Particle Multiplicity Distributions

Multiplicity measurements at relativistic energies have been performed by several experiments using a variety of different detectors, like emulsions, streamer chambers, silicon pad detectors and streamer tube arrays. A unique feature of the WA80 experimental setup is the close to 4π acceptance for charged particle multiplicity measurements combined with the very high statistics allowing small variations to be detected in an analysis of different reaction systems. High statistics is also required for a detailed analysis and understanding of small intermittency phenomena, as reported by Bloomer *et al.* on this conference [9].

Several corrections were applied to the multiplicity data. Some background comes

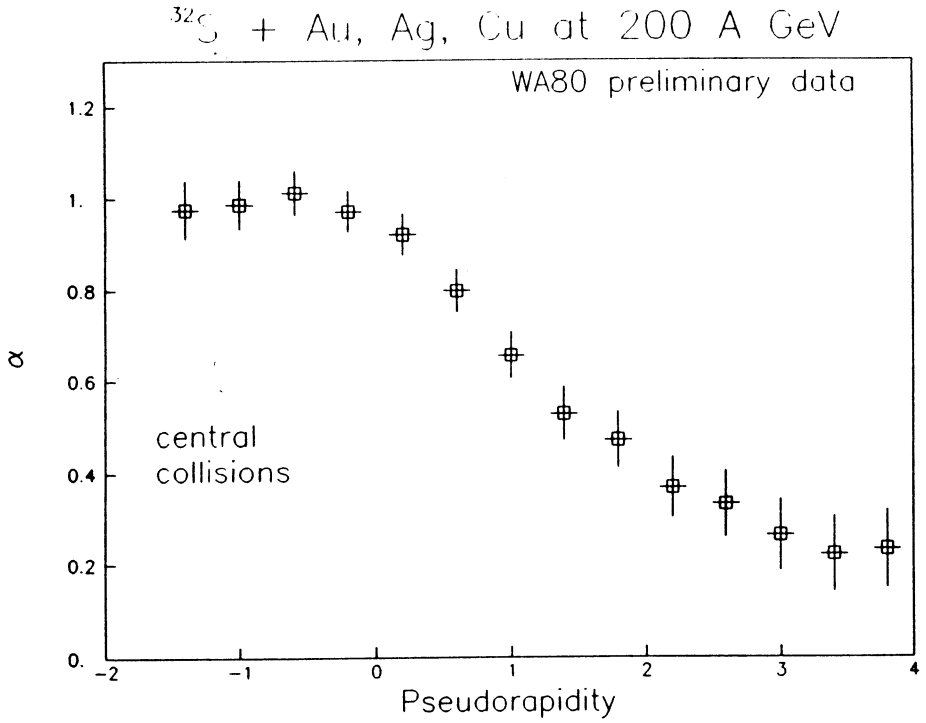

Figure 5: Target mass dependence of the yield of particles as a function of pseudorapidity.

from both real particles and from noise in the electronics and detectors. Real particles may be produced in secondary interactions with the setup but can also come from the unavoidable beam halo, albedo neutrons from the calorimeters, and from cosmic rays. Further corrections include detection efficiencies and multiple hit corrections and are discussed in Ref. [10].

Multiplicity distributions for charged particles from ^{32}S + Al, Cu, Ag, and Au interactions at 200 AGeV are shown in figure 4. As the target gets bigger and the thickness of the nuclear matter to traverse increases, the total multiplicity also increases. The shape of the multiplicity distributions is again dominated by the reaction geometry and resembles very much the shape of the transverse energy distributions. The pseudorapidity distributions, $dN_{ch}/d\eta$, have been analyzed in a similar way as the $dE_T/d\eta$ distributions by fitting a Gaussian distribution to the experimental data in $0.0 < \eta < 4.0$. The target fragmentation region in $-1.7 \leq \eta \leq 0.0$ has been excluded from these fits because the particle density was too high high to get a good description of all data by a single Gaussian (see also next section). As a result we find increasing charged particle densities with increasing target mass and centrality. The largest value of $dN_{ch}/d\eta|_{max} \simeq 175$ per unit rapidity interval is reached in the most central collisions of S + Au. The peak position, $\overline{\eta}$, is found to shift backwards in rapidity with increasing target mass and centrality with the only exception of S + Al where the peak position moves forward with increasing centrality as is due to the inverse reaction kinematics. The width, σ, is found to narrow with increasing centrality and decreasing target mass.

The target mass dependence on the yield of particles as a function of pseudorapidity is shown in Fig. 5 for central collisions. The yield is assumed to follow a power-law

behaviour on the target mass number A_t, i.e. $dN_{ch}/d\eta \propto A_t^{\alpha}$, where α is determined as a function of pseudorapidity. The value of $\alpha \simeq 1$ in the target fragmentation region indicates a strong excitation of the target matter, i.e. the whole target nucleus participates in the reaction, as may be due to rescattering phenomena (see below). At mid-rapidity ($\eta \approx 2.8$) a value of $\alpha \simeq 1/3$ is found which supports the validity of the simple geometrical picture in this region.

4 The Target Fragmentation Region

The results of the charged particle multiplicity analysis (see e.g. Fig. 5) have already demonstrated a strong participation and excitation of the target nucleus in heavy-ion collisions at SPS energies. Having the advantage of a powerful detector for the target fragmentation region, the Plastic-Ball, we will investigate these effects now in more detail by studying the rapidity and transverse momentum distributions of identified baryons, as well as by correlations among positive pions.

4.1 Pseudorapidity Distributions of Protons in p-Nucleus Reactions

High energy pA collisions should provide a first test of different models in the target fragmentation region; models without rescattering or without cumulative effects should show almost no protons at backward angles, because they neglect the influence by the surrounding 'spectator'-matter. We have thus compared pseudorapidity distributions of proton-like fragments ($N_{p\text{-like}} = N_p + N_d + N_t + 2 \cdot N_{\mathrm{He}}$) from p-nucleus collisions for $-1.7 \leq \eta \leq 1.0$ with the Monte-Carlo event generator VENUS 3.07 [11]. This model incorporates rescattering among strings, secondaries, and spectators in a phenomenological way by introducing a reinteraction radius for meson- and baryon-like strings. Rescattering occurs if any two of these objects come closer than the reinteraction distance. We have tuned the model to reproduce the measured proton yields in 200 AGeV p + Au collisions by increasing the baryon reinteraction distance from the default value of 1.4 fm to 1.7 fm and leaving the meson reinteraction distance unchanged at 0.7 fm. With these parameters the distributions for all targets are rather well reproduced, as can be seen from Fig. 6.

While this model can account for the global features of the proton yields with only minor modifications, the exact shape of the kinetic energy spectra is not reproduced. VENUS underestimates the proton yield at very backward angles and overestimates their mean transverse momentum. Recent RQMD calculations [12], on the other hand, are found to underestimate the slope of the spectra somewhat, so that the data appear to fall between the predictions by the two models.

More details on the target mass dependence of proton and pion yields as well as observations of azimuthal correlations among proton and pions, suggesting pion absorption phenomena, are reported in the contribution by Schmidt, *et al.* to this conference [13].

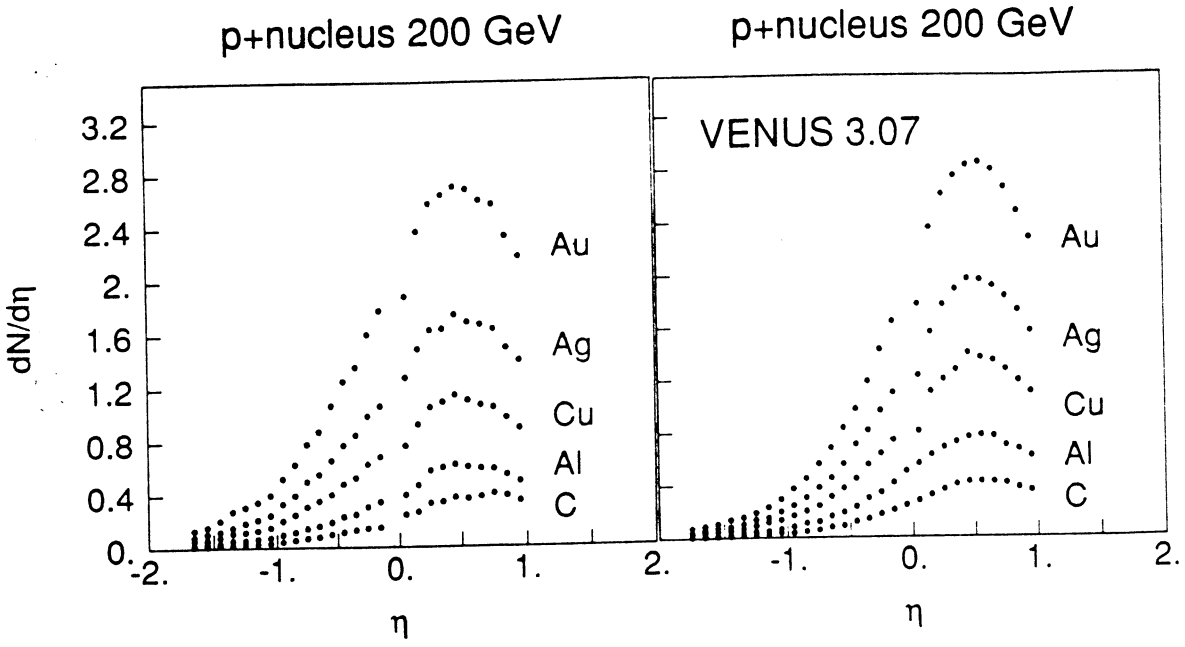

Figure 6: Pseudorapidity distributions of protons measured with the Plastic-Ball (left) and from VENUS 3.07 simulations (right) with modified rescattering parameters.

4.2 Two-Pion Correlations Studies

Further understanding on the space-time development of nucleus-nucleus collisions may be deduced from pion interferometry. We have measured $\pi^+\pi^+$ correlations in the rapidity region $-1.0 \leq y_{\rm lab} \leq 1.0$ for p, ^{16}O, and ^{32}S induced reactions on various nuclei at a bombarding energy of 200 AGeV. The pion source radii have been extracted with a Lorentz-invariant parametrization and are complemented by measurements of the transverse- and longitudinal radii.

A surprising result of the analysis is that the source radii are found to decrease with increasing target mass for the oxygen induced data [14]. The transverse radius for the C-target ($R_T \simeq 3.7$ fm) is larger than the size of the involved nuclei, indicating transverse expansion prior to freeze-out. The values decrease for the heavier targets down to $R_T \simeq 2.4$ fm for O + Au, which is comparable to the size of the projectile. The source sizes for the Au target have been studied also for p- and ^{32}S projectiles at the same bombarding energy per nucleon. For sulfur induced reactions we in fact find a rise to $R_T \simeq 3.2$ fm, which is comparable to the growth of the projectile size. The radius for proton induced reactions is found to be $R_T \approx 2.0$ fm. This value is intermediate between those of the two existing data sets on hadron nucleus interactions at comparable energies [15,16].

While the projectile dependence leads to a variation of the source radii as one might expect intuitively, there remains the question of how to understand the variation of the parameters in case of different targets as studied for oxygen induced reactions. From the analysis discussed in the previous section we found indications for strong rescattering effects in the target region. It is then easy to realize that pions observed in the detector

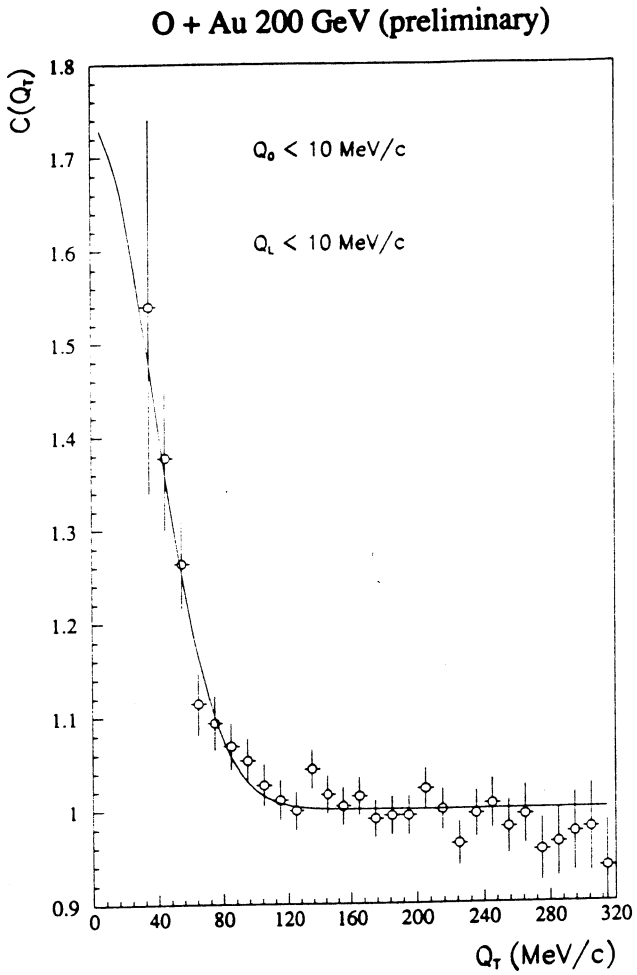

Figure 7: Two pion correlation function for Q_L and $Q_0 \leq 10$ MeV/c in ^{16}O + Au reactions. The solid line represent a fit to a Gaussian source with $R_T \simeq 5.2$ fm.

might undergo very different evolutions; they may be directly produced by participant nucleons traversing the target without further interaction, or they may be rescattered in the target spectator matter after their production. Such a rescattering would alter the volume measured by interferometry to the freeze-out volume of the excited spectator matter. The rescattered pions might come from very large volumes or later times, and their correlation could thus be hidden at very small values of Q, hardly accessible to experiment. It can in fact be demonstrated by simulations [14] that a decrease in the apparent radius may be caused by an interplay of two different sources, where the smaller source is fixed at the projectile radius and the size of the second source grows to large values.

In a more detailed analysis of the reaction O + Au such a large radius can indeed be observed. The correlation function of Q_T for $Q_L \leq 10$ MeV/c and $Q_0 = |E_1 - E_2| \leq 10$ MeV is shown in Fig. 7 together with a Gaussian fit which yields $R_T = (5.2 \pm 0.1)$ fm and $\lambda = 0.74 \pm 0.13$. Similar results can be obtained from a two component fit to the unbiased correlation function [14].

5 Photon and Neutral Pion Spectra

Transverse momentum distributions of produced particles have revealed characteristic differences to a straightforward extrapolation from nucleon-nucleon to nucleus-nucleus

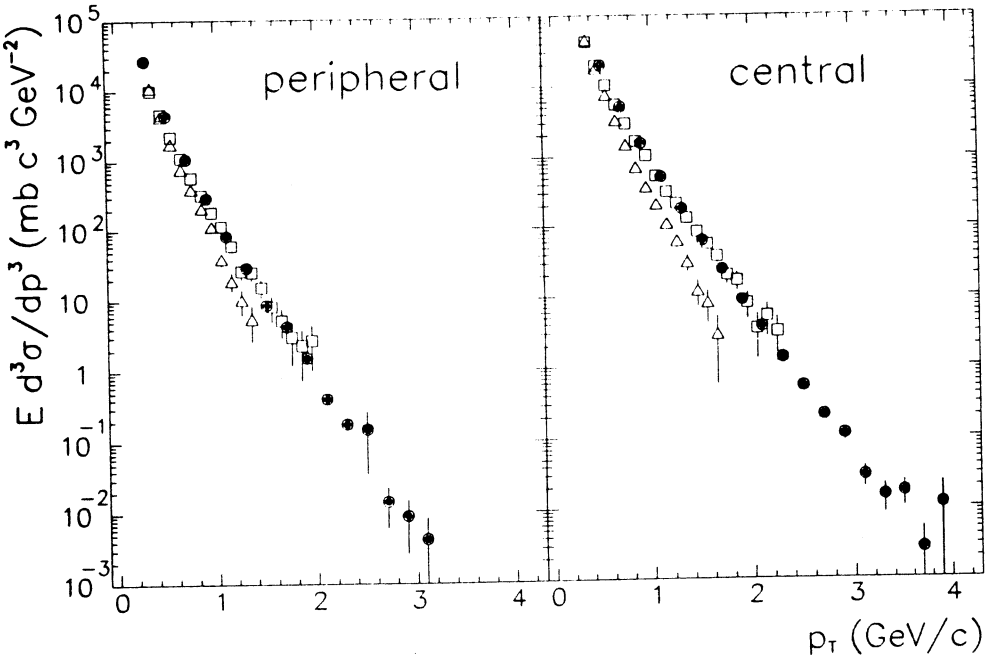

Figure 8: Peripheral and central $\pi^0 p_T$-spectra from 200 AGeV ^{16}O + Au collisions. The black circles denote the experimental data, the open squares (triangles) VENUS 3.07 data with (without) rescattering.

collisions. These differences were observed both in the slope of the p_T-spectra, as well as in their centrality dependence. To examine possible explanations of those deviations we have performed a systematic comparison of inclusive photon- and π^0 p_T-spectra to predictions of the VENUS 3.07 event generator.

Figure 8 shows the experimental π^0 p_T-distributions for peripheral and central 200 AGeV O + Au events. The neutral pions were reconstructed from the decay photons measured with the highly granulated lead-glass detector Saphir [5] in the pseudorapidity range $1.5 \leq \eta \leq 2.1$. A particular feature, pointing to the occurrence of collective effects, is the significant increase of the inverse slope of the spectra when going from peripheral to central events. Superimposed to the measured data are results from the VENUS model which were subjected to the experimental trigger conditions and acceptance of the detector. All data are in units of absolute cross-sections. The influence of rescattering effects to these spectra is studied by switching the rescattering mechanism in the model *on* and *off*, respectively. The spectra with the reinteraction turned *off* were found to resemble very much the predictions of the FRITIOF 1.6 model.

In peripheral collisions there is only very little difference between the two model predictions and both provide a rather good description of the experimental data (see Fig. 8). However, deviations become substantial for central collisions. Here, the simulated p_T-spectrum with rescattering turned *off* results in a too steep distribution as compared to the experimental data. Turning the rescattering mechanism *on* results in a flattening of the spectra so that they become comparable to the experimental data with only a slight excess of particles at large transverse momentum. The same findings as for the π^0-spectra are obtained from the spectra of inclusive photons.

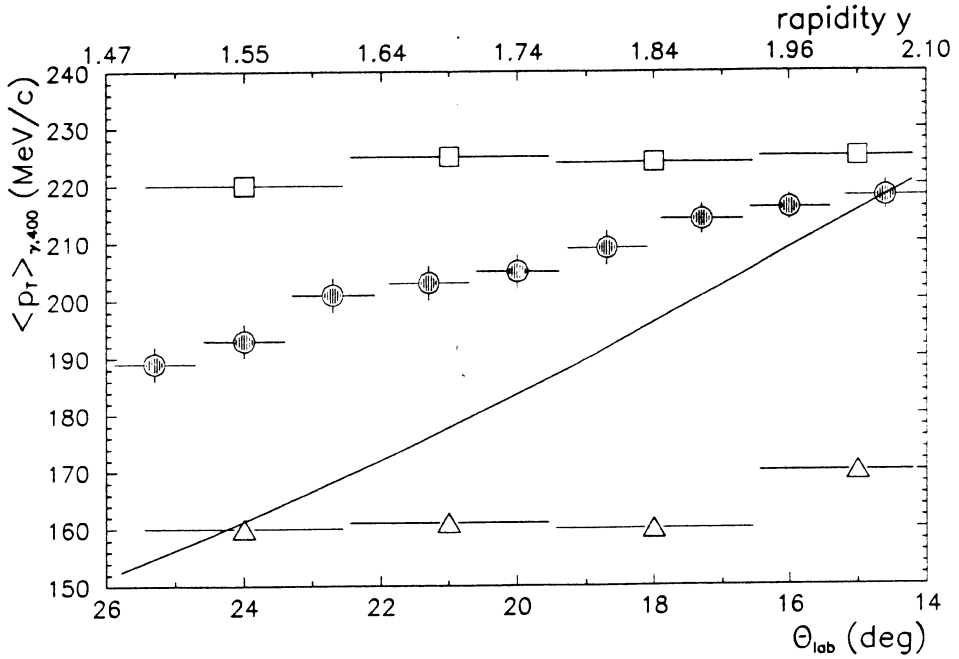

Figure 9: $\langle p_T \rangle_{\gamma,400}$ as a function of the laboratory angle $\theta_{\rm lab}$ and of the rapidity y for central collisions of 200 AGeV ^{16}O + Au. Symbols are as in Fig. 6. Included as a line is also the dependence as expected from an isotropically decaying fireball according to the relation $\langle p_T \rangle_{\gamma,400}(y) \propto 1/\cosh(y_{cm} - y)$.

The observed change in the slopes can be analyzed in an alternative way by calculating the *truncated mean transverse momentum*, defined as

$$\langle p_T \rangle_{\gamma,c} = \frac{\int_c^\infty p_T \frac{dN}{dp_T} dp_T}{\int_c^\infty \frac{dN}{dp_T} dp_T} - c \, .$$

In case of pure exponential distribution the formula leads to exactly the same result as the extraction of the inverse slope parameter. The cutoff momentum has been chosen to be c = 400 MeV/c in order to specifically study the behaviour at large values of p_T. Plotting $\langle p_T \rangle_{\gamma,400}$ as a function of the forward energy, E_{ZDC}, i.e. as a function of the centrality of the collisions, in fact exhibits a rise of the transverse momentum from about 185 MeV/c to 215 MeV/c when going from the most peripheral to the most central events. The behaviour is qualitatively described by the model with rescattering while no variation with the impact parameter is observed with the rescattering mechanism turned *off*.

More information can be obtained by examining the rapidity dependence of the truncated mean transverse momentum as shown in Fig. 9. We find a rise in $\langle p_T \rangle_{\gamma,400}$ by about 15% when approaching mid-rapidity from y = 1.5 to y = 2.1. Now *both* predictions from the VENUS event generator fail to describe the data; the model predicts no rapidity dependence of the mean transverse momentum in the region covered by the experiment. Also included in this plot is the rapidity dependence of $\langle p_T \rangle$ as expected from an isotropically decaying fireball. The absolute value has been normalized to the experimental data point at $\theta_{\rm lab}$ = 14.5°. This model predicts an increase which

is somewhat steeper than the one measured, and may be interpreted as being due to insufficient stopping (see sect. 3) in the data as compared to the pure fireball model.

Preliminary results for central S + Au reactions show an inverse slope parameter of the π^0 p_T-spectra of $T \simeq 225$ MeV/c, which is about 10% larger as the value extracted for central O + Au reactions [17]. Based on the findings from above, we interpret at least part of this increase caused by the rapidity shift of about 0.6 units between the O- and S-experiment (see sect. 2).

6 Analysis of Direct Photons

The production of thermal direct photons has been investigated in reactions of p and ^{16}O projectiles at 60 and 200 AGeV with C and Au nuclei. The analysis, discussed in Ref. [18], is based on the π^0 reconstruction and sets an upper limit of $\gamma_{\text{direct}}/\pi^0 \leq 15\%$ on the signal for all systems in the p_T range of 0.4 GeV/c $\leq p_T \leq$ 2.8 GeV/c. Considering the different sources of errors we expect that the uncertainty of the γ/π^0 ratio can be reduced to 7% or less for the 200 AGeV S + Au data. The largest improvement originates from the much better statistics and from the larger detector coverage improving particularly the acceptance for η mesons. Further gain in experimental sensitivity is expected from an optimized cluster algorithm [19], improving the photon reconstruction efficiency, as well as from advanced procedures to determine the absolute value of the photon reconstruction efficiency as a function of particle density.

The data analysis is presently underway and its results will be presented in the near future.

7 Summary and Conclusions

We have shown that the gross features of ultra-relativistic heavy-ion collisions can be understood in a simple participant spectator picture with the number of participants being the relevant physical quantity to describe the energy and particle flow of the fireball around mid-rapidity. The effect of rescattering shows up in very different measurements. While the global observables are only marginally affected, the effects are most prominent in the target fragmentation region, but show up also in the π^0-spectra close to mid-rapidity and at large values of p_T. It is obviously necessary to include rescattering effects in model calculations to achieve a realistic description of the reaction. All details of the experimental data, like the very backward proton rapidity distributions, or the rapidity dependence of the $\langle p_T \rangle$ of particles are, however, not explained by the models available at present. The results from pion interferometry in the target region can be explained by a two component picture with a very large second component, which again points to effects like rescattering.

Both, the accuracy of the experimental data, as well as the quality of the models have improved considerably in recent times, so that getting down to such 'second order' problems – being ignored initially – seems appropriate. Such an understanding of the variety of effects in dense hadronic matter is mandatory before any final conclusions

about the QGP phase transition can be made.

Partial support by the West German BMFT, GSI, the United States DOE, the Swedish NFR, and the CERN PPE Division is gratefully acknowledged.

References

[1] See this volume and most recent Quark Matter proceedings; Nucl. Phys. **A525** (1991), Nucl. Phys. **A498** (1989), Z. Phys. **C38** (1988).

[2] R. Albrecht, et al., WA80 Collaboration, Report No. GSI-85-32.

[3] G.R. Young, et al., Nucl. Inst. Meth. **A279** (1989) 503.

[4] T.C. Awes, et al., Nucl. Inst. Meth. **A279** (1989) 479.

[5] H. Baumeister, et al., Nucl. Inst. Meth. **A292** (1990) 81.

[6] R. Albrecht, et al., Nucl. Inst. Meth. **A276** (1989) 131.

[7] A. Baden, et al., Nucl. Inst. Meth. **A203** (1982) 189.

[8] R. Albrecht, et al., WA80 Collaboration, Phys. Rev. **C** (1992), in print.

[9] M.A. Bloomer, et al., WA80 Collaboration, proceedings to this conference.

[10] R. Albrecht, et al., WA80 Collaboration, in preparation.

[11] K. Werner, P. Koch, Phys. Lett. **B242** (1990) 251.

[12] H. Sorge, et al., Z. Phys. **C47** (1990) 629.

[13] H.R. Schmidt, et al., WA80 Collaboration, proceedings to this conference.

[14] R. Albrecht, et al., WA80 Collaboration, Z. Phys. **C** (1992) in print.

[15] C. De Marzo et al, Phys. Rev. **D29** (1984) 363.

[16] F. Botterweck, et al., Z. Phys. **C51** (1991) 37.

[17] R. Albrecht, et al., WA80 Collaboration, Z. Phys. **C47** (1991) 367.

[18] R. Albrecht, et al., WA80 Collaboration, Z. Phys. **C51** (1991) 1.

[19] F. Berger, et al., submitted to Nucl. Instr. Meth.